Enhancing Aqueous Carbonation via Co-milled Serpentine and Wollastonite: Effects of Mechanochemical Activation

Hang Zhai,[a,b,*] Qiyuan Chen,[b] Bin Liu,[c] and Bu Wang[b,*]

[a] College of Resources and Environment, Interdisciplinary Research Center for Agriculture Green Development in Yangtze River Basin, Southwest University, Chongqing 400716, China;

[b] Department of Civil and Environmental Engineering, University of Wisconsin-Madison, Madison, Wisconsin 53706, United States;

[c] National Academy of Agriculture Green Development, College of Resources and Environmental Sciences, China Agricultural University, Beijing 100193, P. R. China

[*]**To whom correspondence should be addressed.**

Hang Zhai

College of Resources and Environment, Interdisciplinary Research Center for Agriculture Green Development in Yangtze River Basin, Southwest University, Chongqing 400716, China; orcid.org/0000-0002-8161-448X;

Email: hzhai2024@swu.edu.cn

Bu Wang

Department of Civil and Environmental Engineering, University of Wisconsin-Madison, Madison, Wisconsin 53706, United States;

orcid.org/0000-0002-9294-0918;

Email: bu.wang@wisc.edu

Highlights:

- Co-milled serpentine and wollastonite enhanced aqueous carbonation.
- Without ball milling, the carbonation of serpentine and wollastonite mixtures proceed via forming the combination of $MgCO_3$ and $CaCO_3$.
- The co-milling merged Ca-rich wollastonite with Mg-rich serpentine, leading to the formation of (Mg, Ca)CO_3 after carbonation.
- The aqueous carbonation occurred at the mineral-water interface rather than in the carbonating solutions.

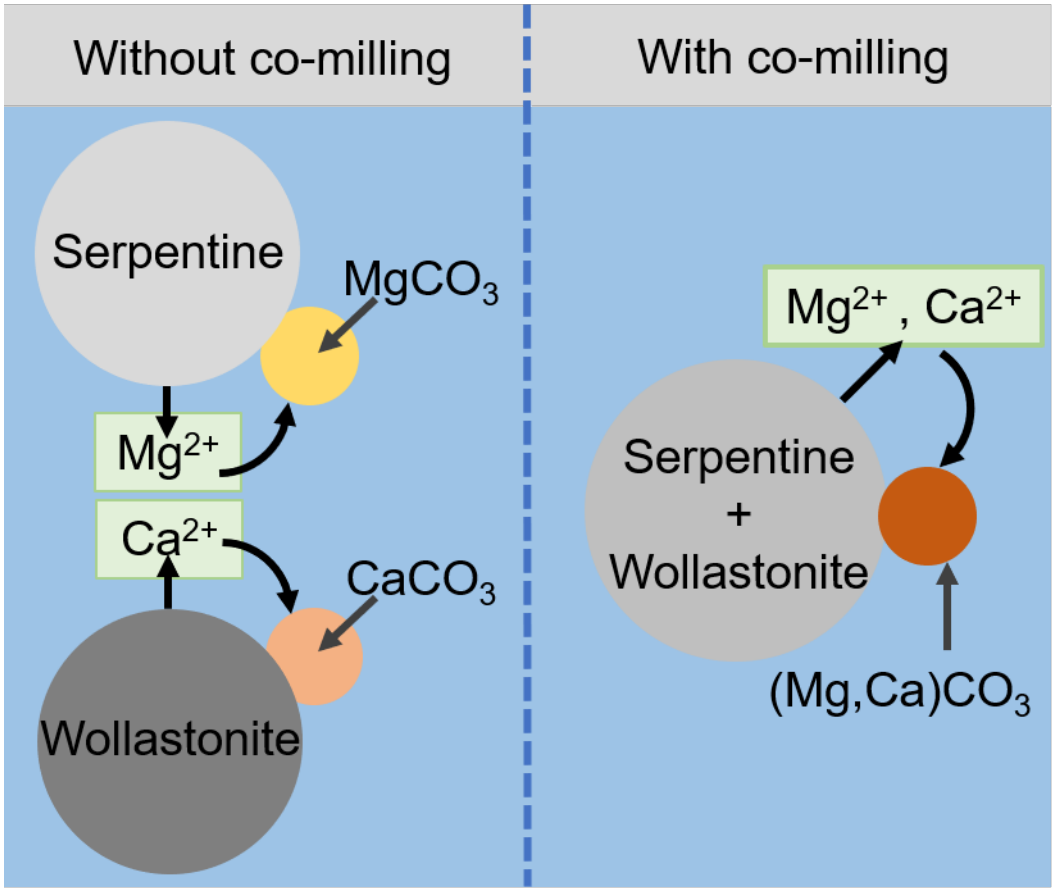

Graphical abstract

Abstract

Carbon dioxide (CO_2) storage through aqueous mineral carbonation is recognized as a promising technology for geochemical carbon removal. Previous studies predominantly focused on individual alkaline earth silicates, such as wollastonite or serpentine, overlooking their interactive effects on carbonation processes. To address this knowledge gap, we conducted aqueous carbonation tests using individually ball-milled serpentine (m-serpentine), wollastonite (m-wollastonite), mixtures of ball-milled serpentine and wollastonite (m-serpentine + m-wollastonite), and the co-milled serpentine and wollastonite (m-(serpentine + wollastonite)). The carbonation of (m-serpentine + m-wollastonite) involved the formation of a combination of calcite ($CaCO_3$) and magnesite ($MgCO_3$), suggesting that no significantly interactive effect between the serpentine and wollastonite. In contrast, carbonating m-(serpentine + wollastonite) results in the precipitation of Mg-bearing calcite ((Mg, Ca)CO_3). Upon quantification, the carbonation degrees of m-(serpentine + wollastonite) is relatively higher than that of (m-serpentine + m-wollastonite). During the carbonation of m-(serpentine + wollastonite), the combination of serpentine and wollastonite facilitates mutual dissolution, leading to the release of more cations. However, these released ions do not diffuse into the bulk carbonating solution; instead, carbonation occurs exclusively at the mineral-water interface. Consequently, the co-milling process, merging Ca-rich wollastonite into Mg-rich serpentine, induces the formation of (Mg, Ca)SiO_3. These novel insights into aqueous carbonation using a combination of Mg-containing and Ca-containing minerals underscore the significant role of mineral-mineral reactions in CO_2 mineralization.

Keywords: aqueous mineral carbonation; wollastonite; serpentine; interfacial coupled dissolution-reprecipitation; ball mill

1. Introduction

The rapid increase in atmospheric carbon dioxide (CO_2), primarily driven by the industrial revolution and extensive fossil fuel usage, has led to the critical issue of global warming (Rosa and Ribeiro, 2001; Smith et al., 2013; Conejo et al., 2020; Yoro and Daramola, 2020). To counteract the rising levels of CO_2 in the atmosphere, mineral carbonation (also known as CO_2 mineralization) stands out as an appealing method. This technology offers advantages such as low financial costs, enhanced reaction kinetics, and secure long-term storage (Romanov et al., 2015; Naraharisetti et al., 2019; Kelemen et al., 2020). In essence, CO_2 mineralization involves chemical reactions between CO_2 and minerals containing elements like Ca, Mg, and Fe, resulting in the formation of thermodynamically stable carbonates like calcite ($CaCO_3$) (Zhai et al., 2023), magnesite ($MgCO_3$) (Santos et al., 2023), and siderite ($FeCO_3$) (Neerup et al., 2023); respectively. Due to the limited availability of natural Ca/Mg/Fe hydroxide and oxide minerals, silicates rich in these elements emerge as promising candidates for CO_2 mineralization (Scott et al., 2021). Wollastonite (Wol, $CaSiO_3$), a representative of Ca-rich silicate minerals, has been extensively studied for its potential in CO_2 long-term storage (Kashim et al., 2020; Feng and Hicks, 2023). In parallel, Mg-rich silicates, particularly serpentine (Ser, $Mg_3Si_2O_5(OH)_4$), have garnered attention due to their abundant deposits and significant capacity for CO_2 storage (Maroto-Valer et al., 2005; Kwon et al., 2011; Eikeland et al., 2015). Additionally, other Ca/Mg-rich silicate minerals, such as plagioclase (Munz et al., 2012; Gudbrandsson et al., 2014), pyroxene

(Monasterio-Guillot et al., 2021), olivine (Wang et al., 2024), and volcanic glasses (Clark et al., 2018), have also been widely utilized for long-term CO_2 storage.

Strategies for CO_2 mineralization utilizing Ca/Mg-rich silicate minerals primarily fall into two categories: *in situ* mineral carbonation processes, involving the direct injection of CO_2 into porous rocks underground (Matter and Kelemen, 2009; Stubbs et al., 2023), and *ex situ* mineral carbonation processes, occurring above ground with pretreatments like rock mining and comminution (Ghoorah et al., 2014; Monasterio-Guillot et al., 2019). When comparing these technologies, *ex situ* mineral carbonation, particularly through the aqueous mineral carbonation route aided by pretreatments, is regarded as the preferred choice to expedite carbonation rates and enhance overall efficiencies (Zhai et al., 2023). Carbonation occurs within an aqueous solution containing dissolved carbonate species through gas-liquid-solid reactions. These reactions accelerate the dissolution of minerals and the precipitation of carbonates (Ragipani et al., 2022). The aqueous carbonation process comprises the dissolution of CO_2 in water (eq. 1), the release of cations (Ca^{2+} or Mg^{2+}) from the mineral matrix (eq. 2 and 3), and the precipitation of carbonates (eq. 4 and 5) (Huijgen et al., 2006; Hövelmann et al., 2011).

$$CO_2\,(g) + H_2O\,(l) \rightarrow H_2CO_3\,(aq) \rightarrow H^+ + HCO_3^- \rightarrow 2\,H^+ + CO_3^{2-} \quad (1)$$

$$Mg_3Si_2O_5(OH)_4\,(s) + 6\,H^+ \rightarrow 3\,Mg^{2+} + 2\,SiO_2\,(s) + 5\,H_2O\,(l) \quad (Ser) \quad (2)$$

$$CaSiO_3\,(s) + 2\,H^+ \rightarrow Ca^{2+} + SiO_2\,(s) + H_2O\,(l) \quad (Wol) \quad (3)$$

$$Ca^{2+} + CO_3^{2-} \rightarrow CaCO_3\,(s) \quad (4)$$

$$Mg^{2+} + CO_3^{2-} \rightarrow MgCO_3\,(s) \quad (5)$$

To augment the degree of aqueous carbonation, strategies primarily concentrate

on promoting the dissolution of carbonating minerals (eq. 2 and 3) and/or the precipitation of stable carbonates (eq. 4 and 5) (Sanna et al., 2014). A common method to accelerate mineral dissolution involves acidifying the solutions, occasionally adjusting salinity and temperature (Orlando et al., 2011; Khan et al., 2023). However, acidic conditions, while aiding dissolution, are unfavorable for carbonates precipitation. Moreover, acidification inhibits the dissolution of CO_2 (eq. 1), leading to the release of CO_2 from aqueous phases. To overcome these challenges, a costly pH swing step is often necessary, involving the addition of bases such as sodium hydroxide (NaOH) or ammonia (NH_3) (Sanna et al., 2013; Azdarpour et al., 2014, 2015). Recently, an alternative approach has been proposed using calcium silicates through an autocatalytic basification process (eq. 6 and 7) (Ragipani et al., 2022; Zhai et al., 2023).

$$CaSiO_3\,(s) + Na_2CO_3\,(aq) + H_2O\,(l) \rightarrow CaCO_3\,(s) + 2\,NaOH\,(aq) + SiO_2\,(s) \quad (6)$$

$$CO_2\,(g) + 2\,NaOH\,(aq) \rightarrow Na_2CO_3\,(aq) + H_2O\,(l) \quad (7)$$

In the carbonation step (eq. 6), the reaction involves soluble carbonates (such as Na_2CO_3) and yields NaOH. Following carbonation, the resulting basic solution can be utilized for CO_2 capture (eq. 7), allowing the regeneration of Na_2CO_3 for reuse in the carbonation process. This approach enables CO_2 mineralization without the need for large pH swings between acidic and basic conditions. All strategies discussed here to enhance mineral carbonation degree primarily revolve around regulating mineral-solution reactions through varying solution conditions. However, an often-overlooked aspect is the role of mineral-mineral reactions during carbonation processes. Recent study has indicated that mixing Ca-bearing and Mg-bearing minerals holds promise for direct atmospheric CO_2 sequestration (Chen et al., 2023). Building on these findings, we infer that the interactive effect between these two minerals could further influence

aqueous carbonation processes. On the one hand, the dissolution of serpentine provides Mg^{2+} ions, which have been shown to inhibit the formation of calcium carbonate nuclei (Zhang and Dawe, 2000; Zhang et al., 2017). Consequently, the addition of serpentine may reduce the carbonation degree of wollastonite. On the other hand, dissolved Mg^{2+} can substitute for Ca^{2+} in calcium silicates (Lothenbach et al., 2015), potentially leading to more Ca^{2+} converting into $CaCO_3$. The net effect of whether wollastonite and serpentine facilitate or inhibit the carbonation of each other remains unknown and warrants further investigation.

While extensive research has been conducted on individual aqueous carbonation processes involving serpentine or wollastonite (McKelvy et al., 2004; Power et al., 2013; Min et al., 2017; Min and Jun, 2018), the interactive effect between these two minerals still remains undisclosed. To address this knowledge gap, we conducted aqueous mineral carbonation experiments under basic conditions, utilizing individually ball-milled serpentine (m-serpentine in manuscript, Ser_m in figures), wollastonite (m-wollastonite in manuscript, Wol_m in figures), mixture of Ser_m and Wol_m (m-serpentine + m-wollastonite in manuscript, Ser_m + Wol_m in figures), co-milled serpentine and wollastonite (m-(serpentine + wollastonite) in manuscript, $(Ser + Wol)_m$ in figures). To our knowledge, previous studies have not explored the role of reactions between carbonating minerals in carbon capture and storage. In this study, we demonstrated that carbonating a mixture of m-(serpentine + wollastonite) led to the formation of Mg-bearing calcite ($(Mg, Ca)CO_3$), distinct from carbonating m-serpentine + m-wollastonite. This highlights the importance of mechanochemical activation in mineral carbonation processes. Our findings shed light on the interactive mechanism between magnesium silicate and calcium silicate minerals under basic carbonation conditions, introducing a novel concept. This approach offers an alternative

method to activate magnesium silicates, with significant implications for improving process efficiency and cost-effectiveness in CO_2 mineralization.

2. Material and methods

2.1 Materials

Natural serpentine (identified as chrysotile) was sourced from California and wollastonite procured from Natural Pigments LLC (CA, USA). X-ray fluorescence (XRF) analyses revealed the composition of the materials (Table S1). Reagent-grade anhydrous sodium carbonate (Na_2CO_3), serving as the CO_2 source, was obtained from Fisher Science. Solutions were prepared using deionized water.

2.2 Ball milling

The high-energy ball milling process was conducted using an 8000M SPEC Certiprep Mixer/Mill (CertiPrep Inc., USA). The particle sizes were measured using a laser diffraction particle size analyzer (~10 μm, Figure S1, LS320, Beckman Coulter, Miami, FL, USA) (*details seen in Supplementary Data*). All samples were characterized using X-ray diffraction (XRD, D8 Discovery, Bruker, Germany) equipped with Cu Kα radiation (λ = 1.54 Å) and operated in the single-axis mode. The divergence, receiving, and anti-scattering slits were set to 0.2 mm, 0.3 mm, and 2 mm, respectively. Data acquisition was performed in four scanning steps from 20° to 60° at a rate of 120 s/step. X-ray photoelectron spectroscopy (XPS) was used to analyze the elemental composition under ultra-high vacuum conditions (5×10^{-10} Torr) with a K-Alpha X-ray photoelectron spectrometer (Thermo Scientific, USA) equipped with a monochromatic Al Kα X-ray source (hν = 1486.6 eV) at 75 W and a detection pass energy of 20-80 eV. The XPS data were processed using Thermal Advantage software (Thermo Scientific, USA) with smart background correction methods and Gaussian functions for peak

fitting (Zhai et al., 2024).

2.3 Aqueous mineral carbonation

Aqueous mineral carbonation was carried out under ambient conditions (25 °C and 0.1 MPa). The mineral carbonation reactions took place in 15 mL polypropylene testing tubes under ambient conditions with vibration, facilitated by a vortex mixer (Fisher Scientific). As the CO_2 source, a 1 M Na_2CO_3 solution (pH = 11, adjusted using 0.1 M NaOH and HCl) was chosen, maintaining a constant liquid-to-solid ratio of 10 mL/g. The reactions were allowed to proceed for 1 hours, and the process was concluded by separating minerals from solutions through 5 minutes of centrifugation (Allegra 25R Centrifuge, Beckman Coulter, USA) at 9000g (Zhai et al., 2024).

2.4 Characterization of carbonated minerals

Carbonated minerals underwent three washes with deionized water to eliminate residual solutions (Zhai et al., 2024). The washed samples were subsequently dried in an Isotemp Oven (model 655F, Fisher Scientific) at 98 °C for 24 hours. Prior to scanning electron microscopy-energy dispersive X-ray (SEM-EDX) analysis, samples were mounted onto Al stubs with Cu tapes and coated with a thin layer of Au (~8 nm, Prep-LeicaACE600 Deposition, Leica, Germany) to enhance electrical conductivity. SEM images were taken under an ultra-high vacuum condition (~10^{-5} Pa) with an acceleration voltage of 10 kV using a secondary electron detector. For nanoscale characterization, high-resolution transmission electron microscope (HRTEM) was employed to directly observe crystallographic phases using FEI Tecnai TF30 TEM (Thermo Fisher Scientific, USA) at a high accelerating voltage of 300 kV (*details seen in Supplementary Data*).

2.5 Quantification of carbonation degrees

The carbonation degree was defined as the conversion of Mg and Ca elements into their corresponding carbonates ($MgCO_3$ and $CaCO_3$). Approximately 15 mg of dry sample was subjected to thermogravimetric analysis (TGA 5500, TA Instruments, USA) under N_2 atmosphere with a gas flow rate of 100 mL/min and a heating rate of 10 °C/min over a temperature range from 30 to 950°C. TGA curves for all samples exhibited three distinct regions: (1) evaporable water loss ($w1$, 30-100°C), (2) bound water loss ($w2$, 100-200°C), and (3) CO_2 release ($w3$, 300-800°C). The stored CO_2 content within the minerals was calculated based on TGA data using the following equation (Zhai et al., 2024):

$$w_{CO_2} = \frac{w_3}{100\% - (w_1 + w_2)} \times 100\% \quad (8)$$

The weight content of converted MgO/CaO (w_{MgO}/w_{CaO}) can be calculated with

$$w_{MgO} = \frac{w_{CO_2}}{M(CO_2)} \times M(MgO) \times 100\% \text{ or } w_{CaO} = \frac{w_{CO_2}}{M(CO_2)} \times M(CaO) \times 100\% \quad (9)$$

in which $M(CO_2)$, M(MgO), and M(CaO) are the molecular weight of CO_2 (44.01 g/mol), MgO (40.30 g/mol), and CaO (55.08 g/mol).

Finally, the conversion of Mg/Ca (C_{Mg}/C_{Ca}) can be calculated by

$$C_{Mg} = \frac{w_{MgO}}{[1-(w_{CO_2}+w_{MgO})] \times \eta_{MgO} + w_{MgO}} \text{ or } C_{Ca} = \frac{w_{CaO}}{[1-(w_{CO_2}+w_{CaO})] \times \eta_{CaO} + w_{CaO}} \quad (10)$$

in which η_{MgO} and η_{CaO} are the weight percent of MgO (40.35%) and CaO (49.27%) within the serpentine and wollastonite.

2.6 Analyses of solution chemistry

The pH of both mineral and mineral-free solutions was measured using an Orion Versa

Star Pro pH/EC meter (Thermo Fischer Scientific, Waltham, Massachusetts, USA). The concentrations of elements within the solutions were determined through inductively coupled plasma optical emission spectrometry (ICP-OES, CCD Simultaneous ICP-OES, VISTA-MPX, Varian, USA) using external standards for calibration. Subsequently, the obtained solutions were acidified and diluted up to 10 times using 0.5 M HNO_3 for dissolved elemental analyses using ICP-OES. All concentrations reported represent the averages of three independent measurements (*details seen in Supplementary Data*).

3. Results

3.1 Mineral carbonation using individually ball-milled serpentine and wollastonite

Spherical serpentine powders (identified as chrysotile, m-serpentine, Ser_m) were obtained by ball milling (Figures 1A and B). The main components of the natural serpentine are 11.71% Fe_2O_3, 40.35% MgO, and 45.89% SiO_2, with a molecular ratio of Fe:Mg:Si at 0.15:1.01:0.76, indicating MgO and SiO_2 as the primary constituents. After reaction, the XRD spectra of carbonated serpentine (c-m-serpentine, C-Ser_m) display a distinctive peak at 32.08°, corresponding to the characteristic peaks of magnesite ($MgCO_3$, Figure 1C). The thermal breakdown of c-m-serpentine occurs at temperatures ranging from 350 to 460 ℃ (Figure 1D), aligning with the thermal decomposition of $MgCO_3$. Quantifying the weight loss from the TGA curve, it is determined that 8.17 wt% of CO_2 is sequestered within c-m-serpentine and the carbonation degree is calculated to be 18.01% after the 1-hour reaction. For individually ball-milled wollastonite powders (m-wollastonite, Figures 1E and F), they comprise 49.27% CaO and 49.67% SiO_2, yielding a Ca/Si mole ratio of 1:1. Acting as a reservoir

for CO_2, wollastonite led to the formation of calcite. The emergence of a new XRD peak, such as the one at 29.49° corresponding to calcite (104) plane (Figure 1G) confirms the transformation of $CaSiO_3$ to $CaCO_3$. The weight loss of carbonated m-wollastonite (c-m-wollastonite, C-wol_m) is prominently observed in the TGA analyses within the temperature range of 500 to 750 °C (Figure 1H). This aligns with the thermal decomposition of $CaCO_3$, setting it apart from the carbonation of m-serpentine. According to TGA curves, approximately 4.1 wt% of CO_2 is sequestered within c-m-wollastonite, resulting in a carbonation degree of 12.89%. This result indicated that the m-wollastonite we used in this study has relatively lower CO_2 storage capacity than that of m-serpentine.

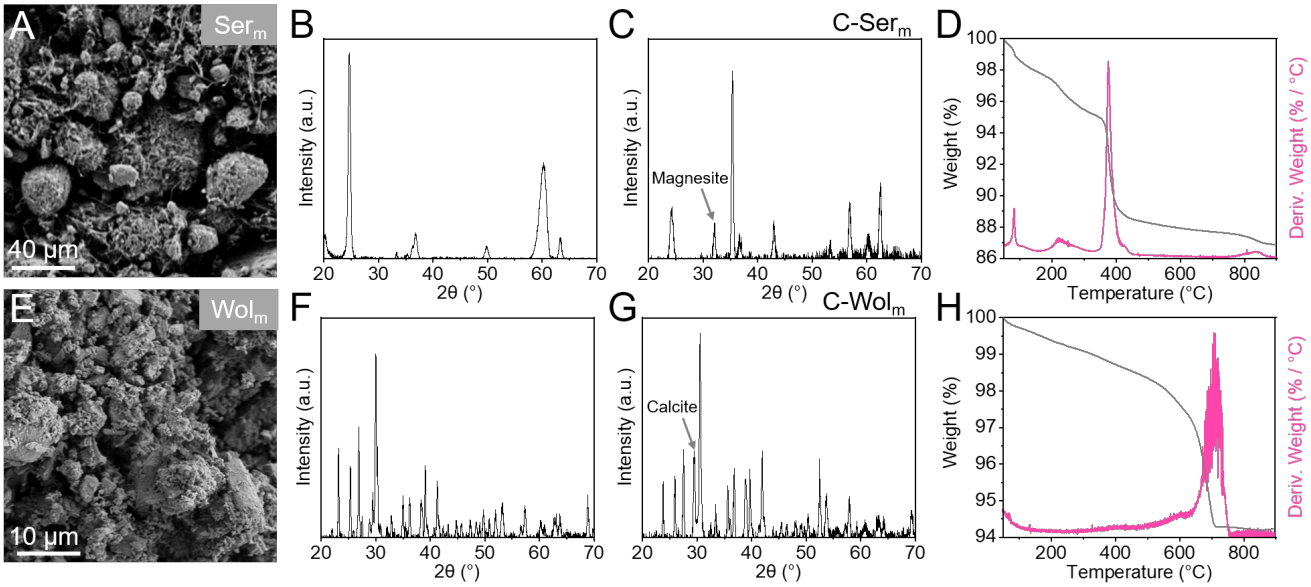

Figure 1. Aqueous mineral carbonation using individually ball-milled (A-D) serpentine (Ser_m) and (E-H) wollastonite (Wol_m). SEM images of individually ball-milled (A) serpentine and (E) wollastonite. XRD spectra of (B and F) serpentine and (C and G) wollastonite before and after carbonation, respectively. TGA curves collected from carbonated (D) serpentine and (H) wollastonite.

3.2 Mineral carbonation using the mixture of individually ball-milled serpentine and wollastonite

To investigate the interactive effect of serpentine and wollastonite on aqueous mineral carbonation, we crafted carbonating materials by directly combining individually ball-milled serpentine and wollastonite (m-serpentine + m-wollastonite, $Ser_m + Wol_m$) powders (Figure 2A). The particle size analyses indicate that the average size of the mixture is approximately 10 μm (Figure S1). Within the mixture, distinct Ca-rich and Mg-rich regions formed with spatial separation (Figures 2C and D), while the Si was the uniformly distributed (Figure 2E). Even after carbonation, c-m-wollastonite and c-m-serpentine remain distinguishable in SEM images (Figure 3A). Carbonated m-serpentine + m-wollastonite (c-(m-serpentine + m-wollastonite), C-($Ser_m + Wol_m$)), exhibits the presence of Ca (Figure 3B), Mg (Figure 3C), and C (Figure 3D). Interestingly, despite reacting in solutions for 1 hour, the Ca and Mg elements do not merge into one phase, still maintaining spatial separation (Figures 3B and C). This result suggested that the carbonation of m-serpentine + m-wollastonite proceeded via the formation of the combination of $MgCO_3$ and $CaCO_3$ rather than (Mg, Ca)CO_3.

To quantify the carbonation degree of the m-serpentine + m-wollastonite mixture, we conducted TGA experiments and the representative weight-temperature curve displayed three distinct weight loss events within temperature ranges of 50-200, 350-460, and 605-710 ℃ (Figure 3E). These events correspond to the evaporation of H_2O, decomposition of $MgCO_3$, and $CaCO_3$, respectively. After separating the decomposition of $MgCO_3$ and $CaCO_3$, we quantified the conversion degree of MgO into $MgCO_3$ and the values increased from 18.87% to 23.12% (Figure 3F). In contrast with the m-serpentine, the carbonation degree of m-wollastonite within the mixture got reduced with increasing the content of m-wollastonite (Figure 3G). Here, the increase or decrease in MgO or CaO conversion degree were influenced by the ration of Na_2CO_3 to serpentine or wollastonite, we will make analyses in the discussion section.

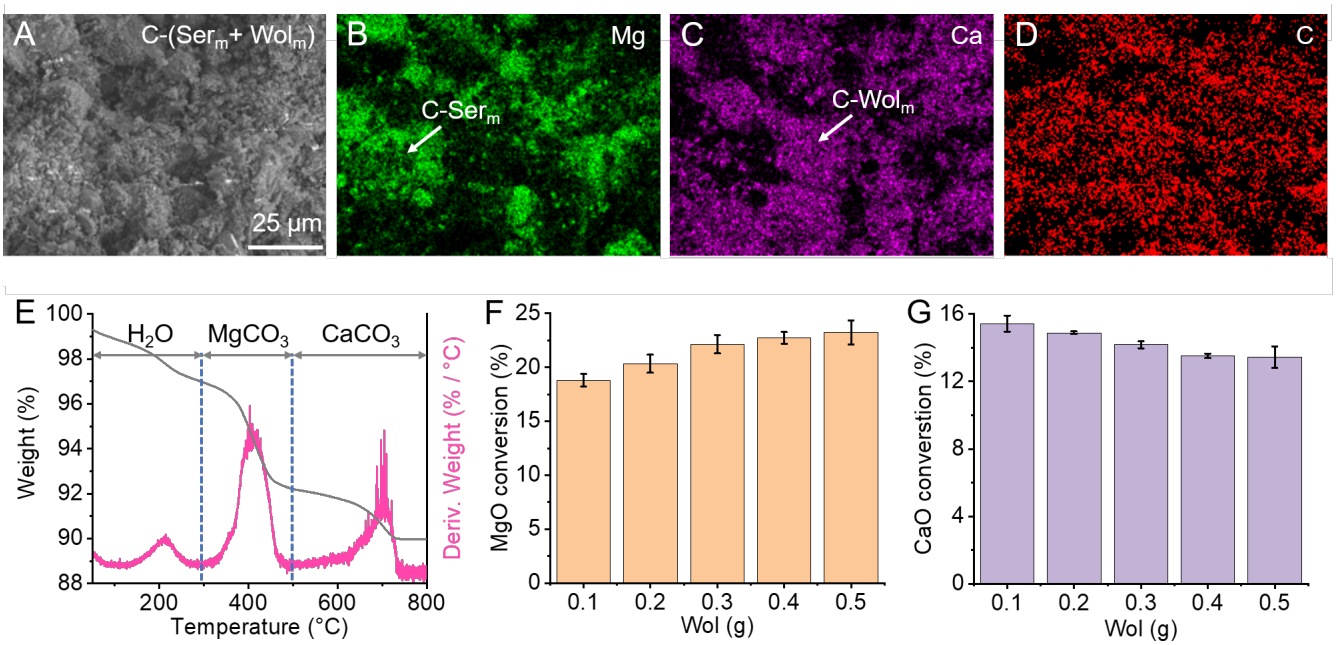

298 **Figure 2.** Preparing and characterizing the mixture of individually ball-milled
299 serpentine and wollastonite (Ser_m + Wol_m). (A) A schematic diagram of preparing
300 sample. (B) A SEM images with corresponding (C) Mg, (D) Ca, and (E) Si distributions.

301

302

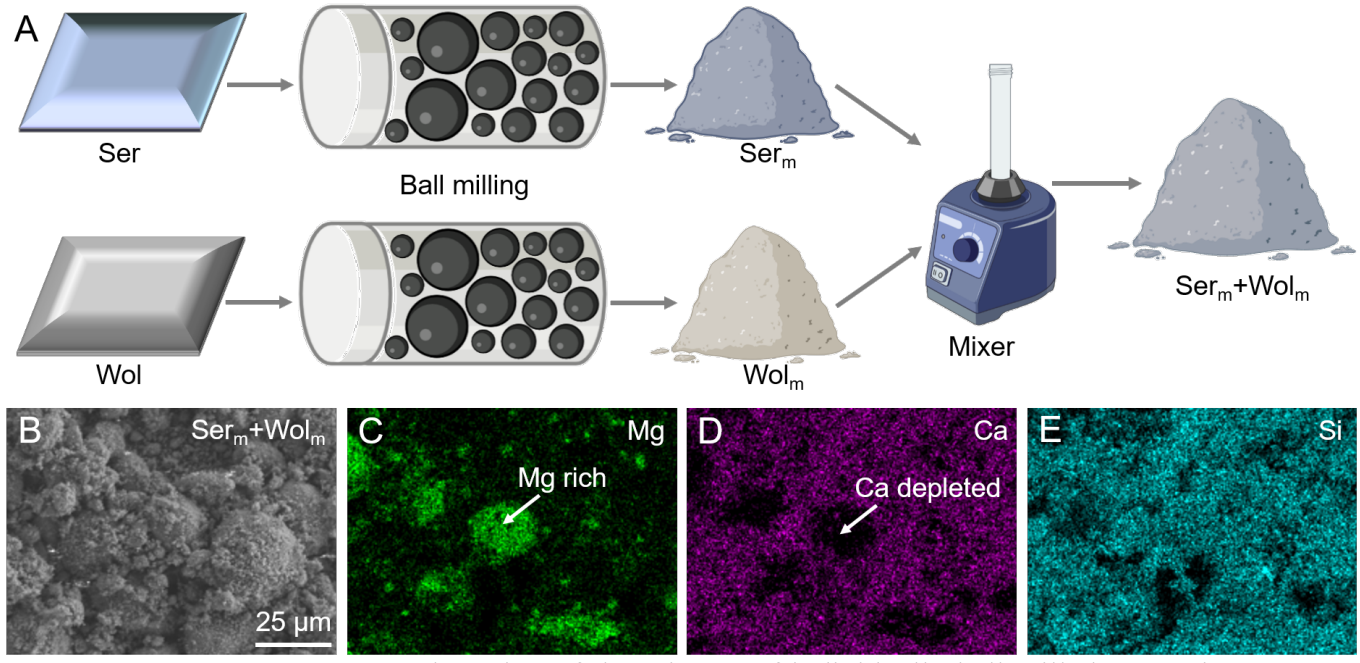

303 **Figure 3.** Aqueous carbonation of the mixture of individually ball-milled serpentine
304 and wollastonite (Ser_m + Wol_m). (A) SEM images and corresponding (B-D) element
305 distributions of C-(Ser_m + Wol_m). (E) A presentative TGA curve indicating the presence
306 of H_2O, $MgCO_3$, and $CaCO_3$ within C-(Ser_m + Wol_m) samples. Quantifications of (F)
307 MgO and (G) CaO within the mixture converting into $MgCO_3$ and $CaCO_3$.

308

3.3 Mineral carbonation using the co-milled wollastonite and serpentine

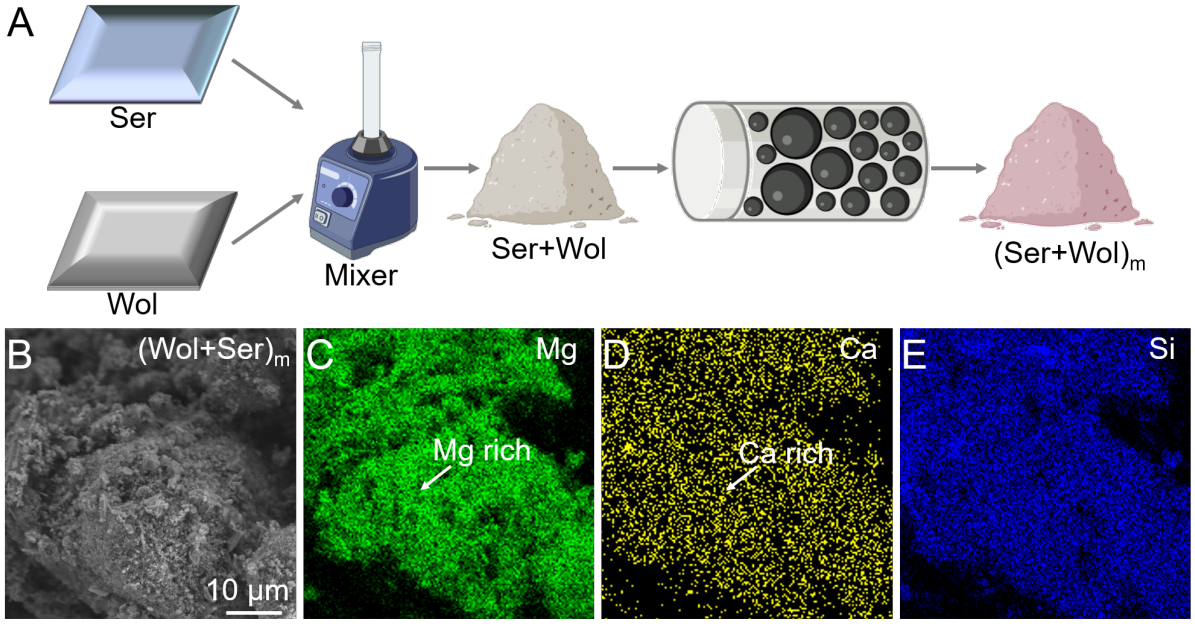

Figure 4. Preparing co-milled serpentine and wollastonite. (A) A schematic diagram of preparing sample. (B) A SEM image with corresponding (C) Mg, (D) Ca, and (E) Si distributions. SEM-EDX results showing wollastonite and serpentine merging into one phase.

Furthermore, we subjected the serpentine and wollastonite mixture to ball milling (Figure 4A). Post co-milling, the original serpentine and wollastonite cannot be discerned through SEM (Figure 4B), and elements (e.g., Mg, Ca, and Si) merge into a single phase (Figures 4C, D, and E). This newly formed phase is referred to as m-(serpentine + wollastonite). Carbonated m-(serpentine + wollastonite), c-m-(serpentine + wollastonite), contains Mg, Ca, Si, and C elements, as revealed by SEM-EDX mapping, showcasing the incorporation of $MgCO_3$ into $CaCO_3$ (Figures 5A, B, C, and D). TGA was employed to quantify the carbonation degree, revealing a single main weight loss event (Figure 5E), distinct from the results of c-(m-serpentine + c-wollastonite). The primary weight loss occurs in the temperature range of 500-700 °C, much higher than that of $MgCO_3$ (Figure 1H) and relatively lower than that of $CaCO_3$ (Figure 1D). As it is challenging to distinguish Ca- or Mg-contributed carbonation, the

CO_2 content is utilized here to represent the carbonation degree. With increasing amounts of wollastonite added into the (m-serpentine + m-wollastonite) mixture, fewer CO_2 molecules were stored within the mixtures (Figure 5F). Since the added wollastonite with low CO_2 storage capacity, the decrease of CO_2 content within the carbonated mixture did not mean that wollastonite inhibited the carbonation of serpentine. Additionally, increasing the amount of wollastonite decreased the specific surface area, resulting in less CO_2 reacting with the minerals (Figure S2). In comparison with (m-serpentine + m-wollastonite), the co-milled samples stored more CO_2, indicating that co-milling enhances the aqueous mineral carbonation of serpentine and wollastonite (Figure 5F).

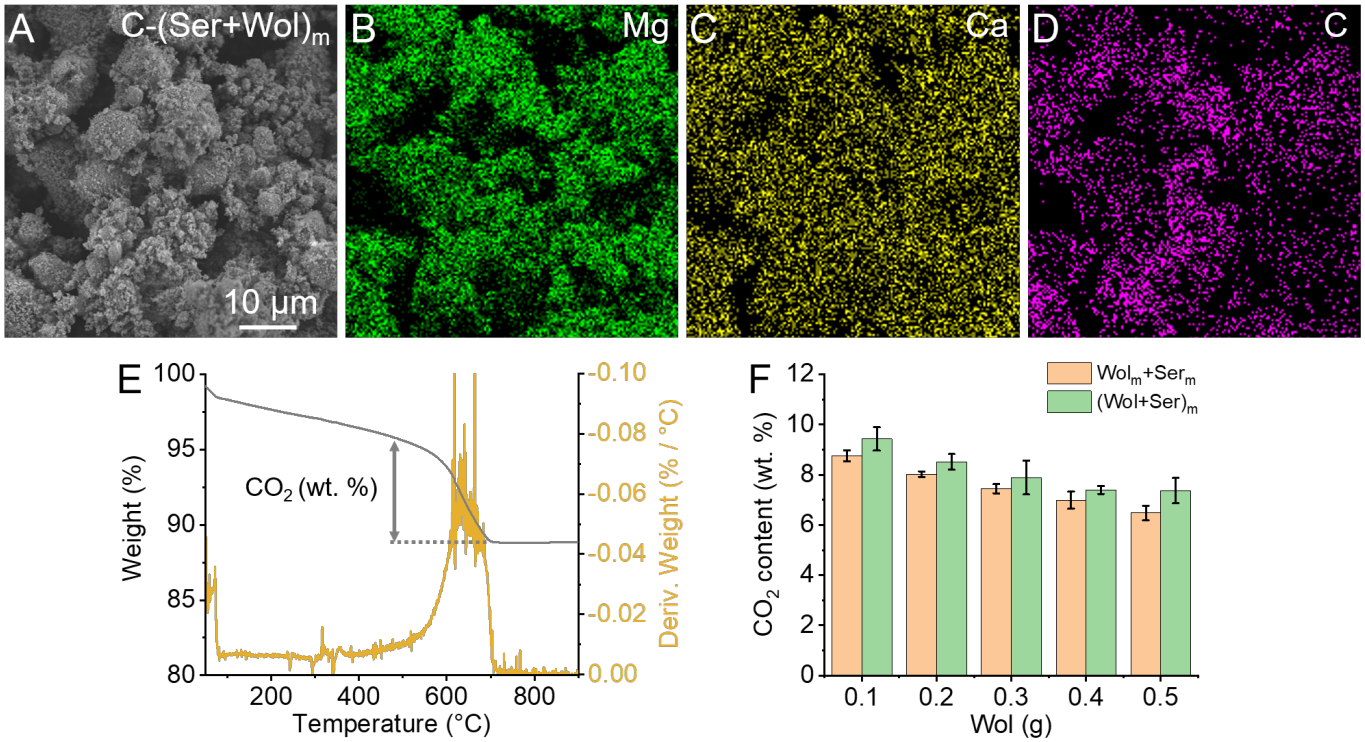

Figure 5. Characterization of carbonated co-milled serpentine and wollastonite (C-(Ser + Wol)$_m$). (A) A presentative SEM image of C-(Ser + Wol)$_m$ samples with corresponding (B) Mg, (C) Ca, and (D) C distributions. (E) A presentative TGA curve showing only one main weight loss step. (F) CO_2 content stored within carbonated (Ser$_m$ + Wol$_m$) (organge bar), and (Ser + Wol)$_m$ (green bar); suggesting that co-milled sample contributes to high carbonation degree than that using the mixed sample.

C-(m-serpentine + m-wollastonite) and c-m-(serpentine + wollastonite) samples exhibit distinct properties, particularly in their thermal decomposition behaviors (Figures 3E and 5E). We attributed the shift in decomposition temperature of c-m-(serpentine + wollastonite) to the formation of Mg-bearing calcium carbonates (Mg, Ca)CO_3. This hypothesis is supported by the presence of Mg, Ca, and C within the single phase (Figures 5A, B, C, and D). To test our hypothesis, we employed XRD to characterize crystalline phases within carbonated samples. In contrast to the XRD spectrum of c-(m-serpentine + m-wollastonite), which contains characteristic peaks of calcite (28.7°) and magnesite (32.8°) (Figure 6A, Figure S3A), the XRD spectrum of c-m-(serpentine + wollastonite) shows no new peaks but an enhanced intensity at 29.8°, corresponding to the Mg-bearing calcite characteristic peak (Figure 6B, Figure S3B). To further identify the newly formed phase at the nanoscale, we imaged the precipitates using TEM (Figure 6D1). The corresponding EDX spectrum demonstrated that the phases consist of C, O, Mg, Si, and Ca elements (Figure 6D2). The high-resolution TEM (HRTEM) image reveals the existence of a crystalline phase (Figure 6D3). Derived from fast Fourier transform (FFT) pattern (Figure 6D4), the measured value of d-spacing is 2.89 Å, close to 3.03 Å for the (104) lattice spacing of calcite. The difference between the measured spacing and the database is attributed to Mg^{2+} (79 pm) substitution for Ca^{2+} (100 pm) in the structure. Combining EDX and HRTEM analyses (Figure 6D), the newly formed phase is identified as Mg-rich calcite, corroborating the XRD and XPS results (Figure 6C1 and C2).

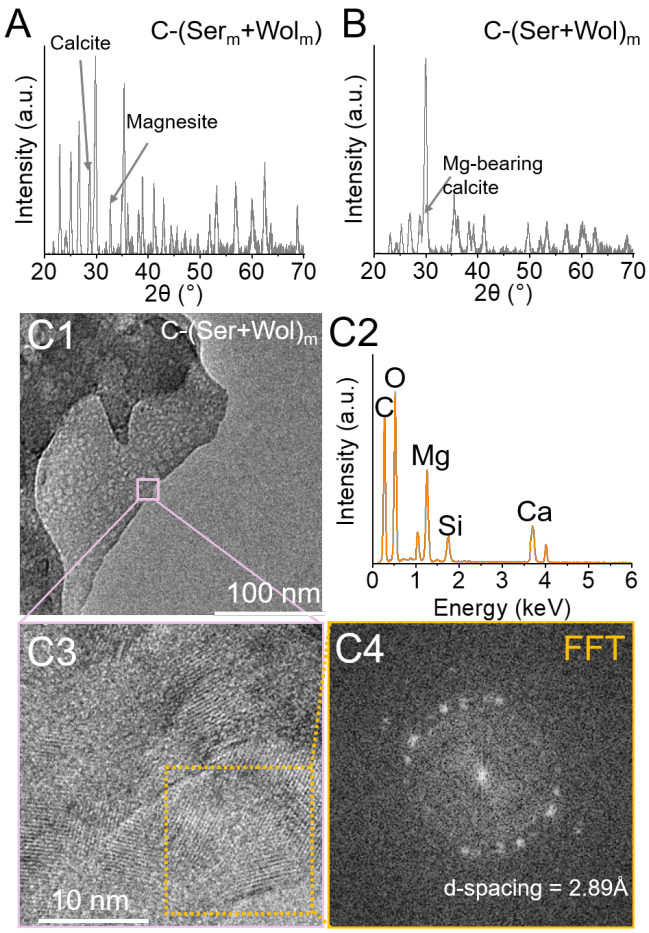

Figure 6. Identifications of new phases within carbonated co-milled serpentine and wollastonite. XRD spectra of (A) C-(Ser$_m$ + Wol$_m$) (as a reference) and (B) C-(Ser + Wol)$_m$. (C1) TEM images of C-(Ser + Wol)$_m$ and (C2) corresponding EDX showing it contains C, O, Mg, Si, and Ca elements. (C3) High resolution TEM (HRTEM) images and corresponding FFT patterns.

4. Discussions

The dissolution of serpentine and wollastonite in carbonate solutions provided a reliable source of cations (Mg^{2+} and Ca^{2+}), subsequently inducing the nucleation and growth of $MgCO_3$ and $CaCO_3$, respectively. $Fe_2(CO_3)_3$ was not detected due to the minimal release of Fe from serpentine (Figure S4). The relatively high concentrations of dissolved silicate inhibited the precipitation of dolomite. Instead, dissolved silicates promoted the incorporation of Mg into Ca-Mg carbonates rather than forming dolomite (Fang and Xu, 2022). Additionally, the Ca to Mg ratio may play a role, as more Ca^{2+} ions were released than Mg^{2+}, which is not thermodynamically favorable for dolomite

formation (Brigatti et al., 2013). Our findings showed that leveraging the synergy carbonation of co-milled serpentine and wollastonite can improve the CO_2 storage (Figure 5F). Similar results have been reported in studies of the carbonation using Mg-based and Ca-based materials. Zhang et al. took insights into the carbonation behavior of $Mg(OH)_2$-$Ca(OH)_2$ mixtures and showed that the carbonation degree increased with the increase of the $Ca(OH)_2$ content (Zhang et al., 2023). Chen et al. showed a similar result that calcite facilitated the carbonation of serpentine (Chen et al., 2023). These results indicated the interaction between two mineral phases endowed the minerals with superior reactivity compared to the single phase. However, in the absent of co-milling, the enhancement of carbonation degree (m-serpentine + m-wollastonite) in this study can be attributed to the different ratios of provided solutions to solid specimens. The increase of wollastonite contents led to a rise in the amount of provided Na_2CO_3 solution, thus promoting the carbonation of both serpentine and wollastonite. Further, we testified the effect of L/S on mineral carbonation, as shown in Figure S4. The carbonation degree of serpentine increased from 18.01% to 23.64% with the rise of the L/S ratio from 10 to 20 mL/g (Figure S5A), demonstrating that increasing water content promoted mineral carbonation. A similar trend was observed in the case of wollastonite (Figure S5B). Therefore, as for the (m-serpentine + m-wollastonite) mixture, the water content provided was higher than that of individually carbonating m-serpentine or m-wollastonite, resulting an increasement in carbonation degree.

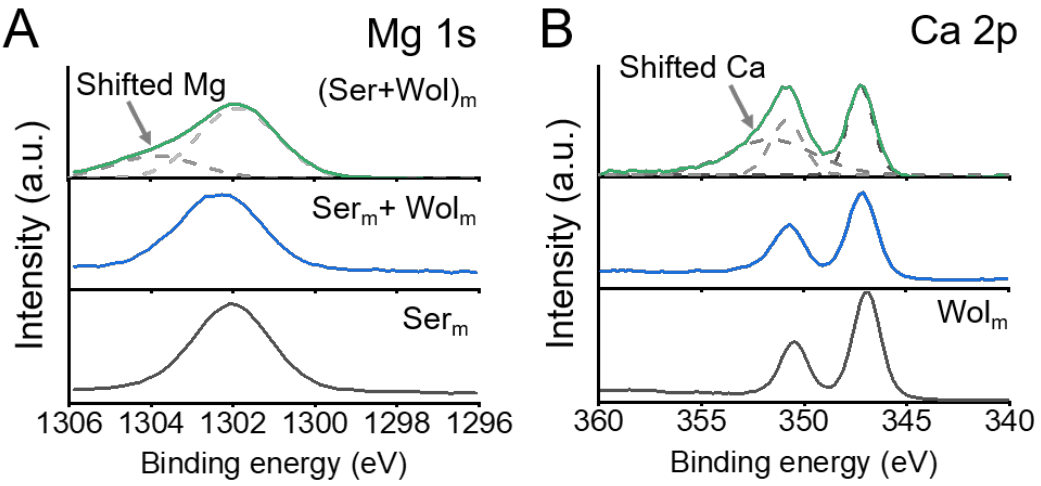

Figure 7. XPS spectra of (A) Mg 1s and (B) Ca 2p and collected from m-serpentine (Ser_m) or m-wollastonite (Wol_m) (black), m-serpentine + m-wollastonite (Ser_m + Wol_m) (blue), and m-(serpentine + wollastonite) $(Ser + Wol)_m$ (green), respectively.

The carbonation degree could be further enhanced with co-milling serpentine and wollastonite. The mixture of serpentine and wollastonite is subjected to high-energy ball-milling operation, inducing various effects, such as solid diffusion, rearrangement of ions/atoms, and atomic intermixing, and subsequently leading to the formation of intermediate phases on the original mineral surface (Maslyk et al., 2022). To explore these effects, we utilized XPS to characterize the states of Mg and Ca elements (Figures 7A and B). Using m-serpentine, m-wollastonite, and m-serpentine + m-wollastonite as references, where Ca 2p1/2 and Ca 2p3/2 are located at 347.1 and 350.7 eV, a new peak at 351.6 eV was identified in the XPS spectrum of m-(serpentine + wollastonite) (Figure 7B). Similar findings were observed in the XPS spectra of Mg 1s (Figure 7A). The simultaneous shifting of Mg 1s and Ca 2p peaks can be explained by the electron attraction between Mg and Ca atoms. Based on our comparative XPS characterizations, we can conclude that the co-milling of serpentine and wollastonite induced a solid-state interfacial reaction with the replacement of ion constituents (e.g. Mg^{2+} and Ca^{2+}) between two mineral surfaces. This interfacial reaction led to the formation of Ca-

containing serpentine and Mg-containing wollastonite phases, which was analogous to the case of co-milled calcite and serpentine. The dissolution of m-(serpentine + wollastonite) released Mg^{2+} and Ca^{2+} ions simultaneously at the mineral-solution interface, contributing to the precipitation of (Mg, Ca)CO_3. Interestingly, compared with (m-serpentine + m-wollastonite), the co-milled minerals released more Mg^{2+} ions from 0.5 g serpentine (Figure 8A). This phenomenon can be interpretated by the divalent metal-promoted dissolution. Released Ca^{2+} competed with Mg^{2+} binding to OH^- or SiO_3^{2-} ions and subsequently limited the reprecipitation of Mg-containing phases (e.g. $Mg(OH)_2$ or $MgSiO_3$), which benefits the dissolution of serpentine. The more Mg^{2+} ions serpentine released into the mineral-solution interface, the higher carbonation degree it got. Here, we still need to note that released Ca^{2+} or Mg^{2+} ions were confined to the mineral-solution interface without diffusion during the carbonation using 1 M Na_2CO_3 (Figure 8B). Consequently, carbonating m-(serpentine + wollastonite) led to the formation of (Mg, Ca)CO_3 since co-milling merged serpentine and wollastonite into a mixture of Ca-containing serpentine and Mg-containing wollastonite.

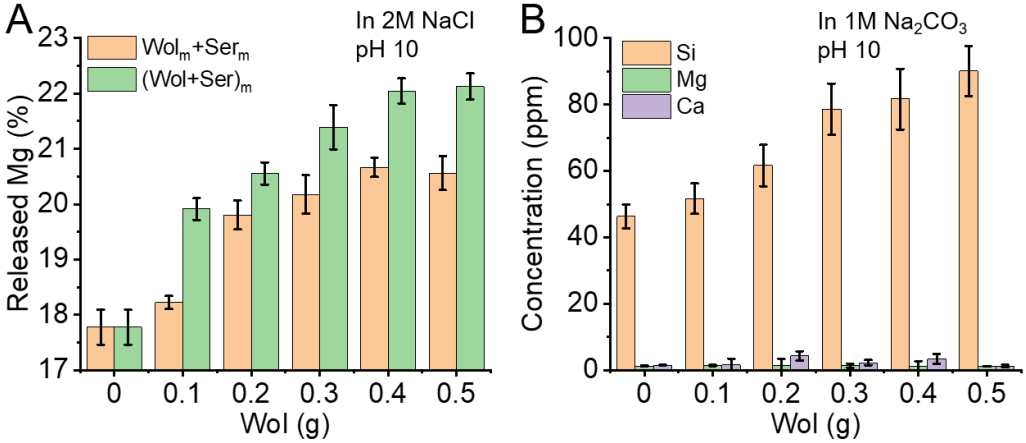

Figure 8. The dissolution properties of m-serpentine + m-wollastonite (Ser_m + Wol_m) and m-(serpentine + wollastonite) $(Ser + Wol)_m$. (A) Quantifications of released Mg from serpentine in the present of 2 M NaCl at pH 10, showing that more Mg^{2+} released from $(Ser + Wol)_m$ than that from (Ser_m +Wol_m). (B) Distribution of elements in solutions during the carbonation using $(Ser + Wol)_m$, showing that released Ca^{2+} or Mg^{2+} ions were confined to the mineral-solution interface without diffusion.

5. Conclusions

In this study, *ex situ* aqueous mineral carbonation was conducted using m-serpentine, m-wollastonite, m-serpentine + m-wollastonite, and m-(serpentine + wollastonite) powders. Through SEM-EDX, TGA-DSC, XRD, XPS, and HRTEM analyses, it was confirmed that carbonation pathways involved the formation of calcite, magnesite, calcite + magnesite, and Mg-bearing calcite for m-serpentine, m-wollastonite, m-serpentine + m-wollastonite, and m-(serpentine + wollastonite), respectively. Quantification revealed that the co-milled sample m-(serpentine + wollastonite) exhibited the highest carbonation degree compared to their equivalent mixture. Our findings underscore the synergistic effect between wollastonite and serpentine on carbonation. These fundamental insights into CO_2-reaction fluid-mineral interactions are crucial for the development of large-scale chemical processes converting CO_2 to carbonates. They also aid in predicting the fate of CO_2 injected into geological formations containing calcium and magnesium silicate minerals and rocks.

Declaration of Competing Interest

The authors declare that they have no known competing financial interests or personal relationships that could have appeared to influence the work reported in this paper.

ACKNOWLEDGEMENTS

This material is based upon work supported by the National Science Foundation under grant no. 2132022. The information, data, or work presented herein were funded in part by the Advanced Research Projects Agency-Energy (ARPA-E), U.S. Department of Energy, under Award Number DE-AR 0001636. The authors gratefully acknowledge use of facilities and instrumentation supported by NSF through the University of Wisconsin Materials Research Science and Engineering Center (DMR-2309000).

Appendix A. Supplementary data

Supplementary data to this article can be found online.

Reference

Azdarpour, A., Asadullah, M., Junin, R., Manan, M., Hamidi, H., Daud, A.R.M., 2014. Carbon dioxide mineral carbonation through ph-swing process: A review. Energy Procedia 61, 2783–2786. https://doi.org/10.1016/j.egypro.2014.12.311

Azdarpour, A., Asadullah, M., Mohammadian, E., Hamidi, H., Junin, R., Karaei, M.A., 2015. A review on carbon dioxide mineral carbonation through pH-swing process. Chem. Eng. J. 279, 615–630. https://doi.org/10.1016/j.cej.2015.05.064

Brigatti, M.F., Galán, E., Theng, B.K.G., 2013. Structure and Mineralogy of Clay Minerals, Developments in Clay Science. https://doi.org/10.1016/B978-0-08-098258-8.00002-X

Chen, M., Zhang, Q., Li, Z., Hu, H., Wang, C., 2023. Insights into the mechanochemical interfacial interaction between calcite and serpentine: Implications for ambient CO2 capture. J. Clean. Prod. 401, 136715. https://doi.org/10.1016/j.jclepro.2023.136715

Clark, A.C., MacFarlane, J., Vanorio, T., 2018. Permeability Evolution of a Cemented Volcanic Ash During Carbonation and CO_2 Depressurization. J. Geophys. Res. Solid Earth 123, 8409–8427. https://doi.org/10.1029/2018JB015810

Conejo, A.N., Birat, J.P., Dutta, A., 2020. A review of the current environmental challenges of the steel industry and its value chain. J. Environ. Manage. 259, 109782. https://doi.org/10.1016/j.jenvman.2019.109782

Eikeland, E., Blichfeld, A.B., Tyrsted, C., Jensen, A., Iversen, B.B., 2015. Optimized carbonation of magnesium silicate mineral for CO_2 storage. ACS Appl. Mater. Interfaces 7, 5258–5264. https://doi.org/10.1021/am508432w

Fang, Y., Xu, H., 2022. Dissolved silica-catalyzed disordered dolomite precipitation. Am. Mineral. 107, 443–452. https://doi.org/10.2138/am-2021-7474

Feng, D., Hicks, A., 2023. Environmental, human health, and CO_2 payback estimation and comparison of enhanced weathering for carbon capture using wollastonite. J. Clean. Prod. 414, 137625. https://doi.org/10.1016/j.jclepro.2023.137625

Ghoorah, M., Dlugogorski, B.Z., Balucan, R.D., Kennedy, E.M., 2014. Selection of acid for weak acid processing of wollastonite for mineralisation of CO_2. Fuel 122, 277–286. https://doi.org/10.1016/j.fuel.2014.01.015

Gudbrandsson, S., Wolff-Boenisch, D., Gislason, S.R., Oelkers, E.H., 2014. Experimental determination of plagioclase dissolution rates as a function of its composition and pH at 22°C. Geochim. Cosmochim. Acta 139, 154–172. https://doi.org/10.1016/j.gca.2014.04.028

Hövelmann, J., Austrheim, H., Beinlich, A., Anne Munz, I., 2011. Experimental study of the carbonation of partially serpentinized and weathered peridotites. Geochim. Cosmochim. Acta 75, 6760–6779. https://doi.org/10.1016/j.gca.2011.08.032

Huijgen, W.J.J., Witkamp, G.J., Comans, R.N.J., 2006. Mechanisms of aqueous wollastonite carbonation as a possible CO_2 sequestration process. Chem. Eng. Sci. 61, 4242–4251. https://doi.org/10.1016/j.ces.2006.01.048

Kashim, M.Z., Tsegab, H., Rahmani, O., Abu Bakar, Z.A., Aminpour, S.M., 2020. Reaction Mechanism of Wollastonite in Situ Mineral Carbonation for CO_2 Sequestration: Effects of Saline Conditions, Temperature, and Pressure. ACS Omega 5, 28942–28954. https://doi.org/10.1021/acsomega.0c02358

Kelemen, P.B., McQueen, N., Wilcox, J., Renforth, P., Dipple, G., Vankeuren, A.P., 2020. Engineered carbon mineralization in ultramafic rocks for CO_2 removal from air: Review and new insights. Chem. Geol. 550, 119628. https://doi.org/10.1016/j.chemgeo.2020.119628

Khan, R.I., Intesarul Haque, M., Siddique, S., Landis, E.N., Ashraf, W., 2023. Effects of amino acids on the multiscale properties of carbonated wollastonite composites. Constr. Build. Mater. 374, 130816. https://doi.org/10.1016/j.conbuildmat.2023.130816

Kwon, S., Fan, M., Dacosta, H.F.M., Russell, A.G., Tsouris, C., 2011. Reaction kinetics of CO_2 carbonation with Mg-rich minerals. J. Phys. Chem. A 115, 7638–7644. https://doi.org/10.1021/jp2040899

Lothenbach, B., Nied, D., L'Hôpital, E., Achiedo, G., Dauzères, A., 2015. Magnesium and calcium silicate hydrates. Cem. Concr. Res. 77, 60–68. https://doi.org/10.1016/j.cemconres.2015.06.007

Maroto-Valer, M.M., Fauth, D.J., Kuchta, M.E., Zhang, Y., Andrésen, J.M., 2005. Activation of magnesium rich minerals as carbonation feedstock materials for CO_2 sequestration. Fuel Process. Technol. 86, 1627–1645. https://doi.org/10.1016/j.fuproc.2005.01.017

Maslyk, M., Gäb, T., Matveeva, G., Opitz, P., Mondeshki, M., Krysiak, Y., Kolb, U., Tremel, W., 2022. Multistep Crystallization Pathways in the Ambient-Temperature Synthesis of a New Alkali-Activated Binder. Adv. Funct. Mater. 32. https://doi.org/10.1002/adfm.202108126

Matter, J.M., Kelemen, P.B., 2009. Permanent storage of carbon dioxide in geological reservoirs by mineral carbonation. Nat. Geosci. 2, 837–841. https://doi.org/10.1038/ngeo683

McKelvy, M.J., Chizmeshya, A.V.G., Diefenbacher, J., Béarat, H., Wolf, G., 2004. Exploration of the role of heat activation in enhancing serpentine carbon sequestration reactions. Environ. Sci. Technol. 38, 6897–6903. https://doi.org/10.1021/es049473m

Min, Y., Jun, Y.S., 2018. Wollastonite carbonation in water-bearing supercritical CO_2: Effects of water saturation conditions, temperature, and pressure. Chem. Geol. 483, 239–246. https://doi.org/10.1016/j.chemgeo.2018.01.012

Min, Y., Li, Q., Voltolini, M., Kneafsey, T., Jun, Y.S., 2017. Wollastonite Carbonation

in Water-Bearing Supercritical CO_2: Effects of Particle Size. Environ. Sci. Technol. 51, 13044–13053. https://doi.org/10.1021/acs.est.7b04475

Monasterio-Guillot, L., Di Lorenzo, F., Ruiz-Agudo, E., Rodriguez-Navarro, C., 2019. Reaction of pseudowollastonite with carbonate-bearing fluids: Implications for CO_2 mineral sequestration. Chem. Geol. 524, 158–173. https://doi.org/10.1016/j.chemgeo.2019.06.011

Monasterio-Guillot, L., Fernandez-Martinez, A., Ruiz-Agudo, E., Rodriguez-Navarro, C., 2021. Carbonation of calcium-magnesium pyroxenes: Physical-chemical controls and effects of reaction-driven fracturing. Geochim. Cosmochim. Acta 304, 258–280. https://doi.org/10.1016/j.gca.2021.02.016

Munz, I.A., Brandvoll, Haug, T.A., Iden, K., Smeets, R., Kihle, J., Johansen, H., 2012. Mechanisms and rates of plagioclase carbonation reactions. Geochim. Cosmochim. Acta 77, 27–51. https://doi.org/10.1016/j.gca.2011.10.036

Naraharisetti, P.K., Yeo, T.Y., Bu, J., 2019. New classification of CO_2 mineralization processes and economic evaluation. Renew. Sustain. Energy Rev. 99, 220–233. https://doi.org/10.1016/j.rser.2018.10.008

Neerup, R., Løge, I.A., Kontogeorgis, G.M., Thomsen, K., Fosbøl, P.L., 2023. Measurements and modelling of $FeCO_3$ solubility in water relevant to corrosion and CO_2 mineralization. Chem. Eng. Sci. 270, 118549. https://doi.org/10.1016/j.ces.2023.118549

Orlando, A., Borrini, D., Marini, L., 2011. Dissolution and carbonation of a serpentinite: Inferences from acid attack and high P-T experiments performed in aqueous solutions at variable salinity. Appl. Geochemistry 26, 1569–1583. https://doi.org/10.1016/j.apgeochem.2011.06.023

Power, I.M., Wilson, S.A., Dipple, G.M., 2013. Serpentinite carbonation for CO_2 sequestration. Elements 9, 115–121. https://doi.org/10.2113/gselements.9.2.115

Ragipani, R., Sreenivasan, K., Anex, R.P., Zhai, H., Wang, B., 2022. Direct Air Capture and Sequestration of CO_2 by Accelerated Indirect Aqueous Mineral Carbonation under Ambient Conditions. ACS Sustain. Chem. Eng. 10, 7852–7861. https://doi.org/10.1021/acssuschemeng.1c07867

Romanov, V., Soong, Y., Carney, C., Rush, G.E., Nielsen, B., O'Connor, W., 2015. Mineralization of Carbon Dioxide: A Literature Review. ChemBioEng Rev. 2, 231–256. https://doi.org/10.1002/cben.201500002

Rosa, L.P., Ribeiro, S.K., 2001. The present, past, and future contributions to global warming of CO_2 emissions from fuels a key for negotiation in the climate convention. Clim. Change 48, 289–307. https://doi.org/10.1023/A:1010720931557

Sanna, A., Dri, M., Maroto-Valer, M., 2013. Carbon dioxide capture and storage by pH swing aqueous mineralisation using a mixture of ammonium salts and antigorite source. Fuel 114, 153–161. https://doi.org/10.1016/j.fuel.2012.08.014

Sanna, A., Uibu, M., Caramanna, G., Kuusik, R., Maroto-Valer, M.M., 2014. A review of mineral carbonation technologies to sequester CO_2. Chem. Soc. Rev. 43, 8049–8080. https://doi.org/10.1039/c4cs00035h

Santos, H.S., Nguyen, H., Venâncio, F., Ramteke, D., Zevenhoven, R., Kinnunen, P., 2023. Mechanisms of Mg carbonates precipitation and implications for CO_2 capture and utilization/storage. Inorg. Chem. Front. 10. https://doi.org/10.1039/d2qi02482a

Scott, A., Oze, C., Shah, V., Yang, N., Shanks, B., Cheeseman, C., Marshall, A., Watson, M., 2021. Transformation of abundant magnesium silicate minerals for enhanced CO_2 sequestration. Commun. Earth Environ. 2, 1–6. https://doi.org/10.1038/s43247-021-00099-6

Smith, K.R., Desai, M.A., Rogers, J. V., Houghton, R.A., 2013. Joint CO_2 and CH_4 accountability for global warming. Proc. Natl. Acad. Sci. U. S. A. 110. https://doi.org/10.1073/pnas.1308004110

Stubbs, A.R., Power, I.M., Paulo, C., Wang, B., Zeyen, N., Wilson, S., Mervine, E., Gunning, C., 2023. Impact of wet-dry cycles on enhanced rock weathering of brucite, wollastonite, serpentinite and kimberlite: Implications for carbon verification. Chem. Geol. 637, 121674. https://doi.org/10.1016/j.chemgeo.2023.121674

Wang, Y., Li, Y., Li, M., Jiao, N., Zheng, Q., Yu, R., Zhang, E., Liu, D., 2024. Influence of alkaline earth metal ions upon the dissolution and carbon storage of olivine containing associated kaolinite. Appl. Clay Sci. 255, 107394. https://doi.org/10.1016/j.clay.2024.107394

Yoro, K.O., Daramola, M.O., 2020. CO_2 emission sources, greenhouse gases, and the global warming effect, Advances in Carbon Capture: Methods, Technologies and Applications. Elsevier Inc. https://doi.org/10.1016/B978-0-12-819657-1.00001-3

Zhai, H., Chen, Q., Duan, Y., Liu, B., Wang, B., 2024. Silica Polymerization Driving Opposite Effects of pH on Aqueous Carbonation Using Crystalline and Amorphous Calcium Silicates. Inorg. Chem. 63, 4574–4582. https://doi.org/10.1021/acs.inorgchem.3c04005

Zhai, H., Chen, Q., Yilmaz, M., Wang, B., 2023. Enhancing Aqueous Carbonation of Calcium Silicate through Acid and Base Pretreatments with Implications for Efficient Carbon Mineralization. Environ. Sci. Technol. 57, 13808–13817. https://doi.org/10.1021/acs.est.3c03942

Zhang, J., Sun, Y., Yu, J., 2017. Qualitative discussion of prenucleation cluster role in crystallization of calcium carbonate under high concentration of magnesium based on experimental phenomena. J. Cryst. Growth 478, 77–84. https://doi.org/10.1016/j.jcrysgro.2017.07.012

Zhang, Y., Dawe, R.A., 2000. Influence of Mg^{2+} on the kinetics of calcite precipitation and calcite crystal morphology. Chem. Geol. 163, 129–138. https://doi.org/10.1016/S0009-2541(99)00097-2

Zhang, Z., Liu, Z., Wang, F., Hu, S., 2023. Elucidating the Interaction Mechanism of $Mg(OH)_2$ and $Ca(OH)_2$ under Enforced Carbonation. ACS Sustain. Chem. Eng. 11, 9442–9454. https://doi.org/10.1021/acssuschemeng.3c01549